

Ultrafast relaxation dynamics of the antiferrodistortive phase in Ca doped SrTiO₃

M. Porer,^{1,*} M. Fechner,^{2,3} E. Bothschafter,¹ L. Rettig,^{1,4} M. Savoini,^{1,5}
V. Esposito,¹ J. Rittmann,¹ M. Kubli,⁵ M. J. Neugebauer,⁵ E. Abreu,⁵ T.
Kubacka,⁵ T. Huber,⁵ G. Lantz,⁵ S. Parchenko,¹ S. Grübel,¹ A. Paarmann,⁴ J.
Noack,⁶ P. Beaud,¹ G. Ingold,¹ U. Aschauer,⁷ S. L. Johnson,⁵ and U. Staub^{1,†}

¹*Swiss Light Source, Paul Scherrer Institute, 5232 Villigen-PSI, Switzerland*

²*Max Planck Institute for the Structure and Dynamics
of Matter, CFEL, 22761 Hamburg, Germany*

³*Materials Theory, ETH Zürich, 8093 Zürich, Switzerland*

⁴*Department of Physical Chemistry, Fritz Haber Institute
of the Max Planck Society, 14195 Berlin, Germany*

⁵*Institute for Quantum Electronics, ETH Zürich, 8093 Zürich, Switzerland*

⁶*Department of Inorganic Chemistry, Fritz Haber Institute
of the Max Planck Society, 14195 Berlin, Germany*

⁷*Department of Chemistry and Biochemistry, University of Bern, 3012 Bern, Switzerland*

(Dated: May 1, 2018)

Abstract

The ultrafast dynamics of the octahedral rotation in Ca:SrTiO₃ is studied by time resolved x-ray diffraction after photo excitation over the band gap. By monitoring the diffraction intensity of a superlattice reflection that is directly related to the structural order parameter of the soft-mode driven antiferrodistortive phase in Ca:SrTiO₃, we observe a ultrafast relaxation on a 0.2 ps timescale of the rotation of the oxygen octahedron, which is found to be independent of the initial temperature despite large changes in the corresponding soft-mode frequency. A further, much smaller reduction on a slower picosecond timescale is attributed to thermal effects. Time-dependent density-functional-theory calculations show that the fast response can be ascribed to an ultrafast displacive modification of the soft-mode potential towards the normal state, induced by holes created in the oxygen 2p states.

* Michael@Porer.org

† Urs.Staub@psi.ch

Understanding the dynamics and speed limits of structural and/or electronic symmetry breakings is fundamental for possible applications in ultrafast data storage. Most studies in condensed matter systems are concerned with electronically driven phase transitions including either charge [1, 2] and orbital orders, [2, 3] charge density wave order [4, 5], magnetic phase transitions [6–9] or magnetization reversal [10, 11]. It is crucial to determine the timescale of these processes as well as the speed at which the crystal structure follows ultrafast modifications of electronic (magnetic) order in the time domain. This has been achieved for correlated materials such as e.g. manganites [2] and VO₂ [12, 13] by using ultrafast x-ray and electron diffraction.

Purely structural phase transitions, however, are solely governed by interactions within the phonon system [14] without any electronic or spin modulation as a driving force. For such transitions, very little is known about the dynamics induced by an electronic excitation.

In the common picture of the two-temperature model [15], phonon driven distortions might be expected to relax on a timescale of a few ps determined by the rate of heat transfer from the electronic to the lattice system. This can be compared to phase transitions driven by coupling to an electronic order parameter, where the structural relaxation is on the order of a few hundred femtoseconds or faster [2].

Pristine SrTiO₃ is an insulating simple cubic perovskite at room temperature and undergoes a prototypical, purely structural phase transition from cubic (spacegroup Pm-3m) to tetragonal symmetry (spacegroup I4/mcm) below $T_c = 105$ K. This transition is solely driven by softening of a mode at the zone boundary [16, 17]. A polar phonon mode softens as well, however, the system remains paraelectric down to the lowest temperatures [18] because quantum fluctuations [19] prevent a ferroelectric phase transition.

The antiferrodistortive structural modulation manifests itself by a rotation of the TiO₆ octahedra by an angle φ (inset of Fig. 1) [16, 17] at a wavevector of $q=R$ (we keep the Pm-3m symmetry for the subsequent discussion). As φ is small, in equilibrium it can be seen as the order parameter of the transition [Mueller]. The modulation gives rise to x-ray superlattice (SL) reflections with intensity approximately proportional to the square of the atomic displacement u of the I4/mcm oxygen 8h sites and to the square of φ (see supplementary material).

Here we employ ultrafast X-ray diffraction to monitor the structural order parameter of SrTiO₃ following ultrafast optical injection of e-h pairs. We find a fast partial relaxation on

a timescale of 0.2 ps. We identify these dynamics as being non-thermally driven by changes of the phonon-potentials induced by oxygen 2p hole doping. The increase of average lattice temperature is found to play a minor role.

The static properties of commercially available single crystals of $\text{Sr}_{0.97}\text{Ca}_{0.03}\text{TiO}_3$ [20] were characterized by hard x-ray diffraction at the Materials Sciences beamline of the Swiss Light Source (SLS) at the Paul Scherrer Institute [21], and by Raman spectroscopy of the octahedral soft mode. We obtain a critical temperature of $T_c = 280$ K and a soft-mode frequency of 2.5 THz at $T = 100$ K (Fig. S1). Isovalent substitution of Sr with Ca in SrTiO_3 leads to an increase of T_c , but does not change the symmetry of the distorted phase for doping levels below 6% [22]. Our choice of 3% of Ca-doping enables us to access the distorted phase via cooling with liquid N_2 .

Approximately 120 fs long x-ray pulses with 7.1 keV energy and 2 kHz repetition rate, available at the FEMTO slicing facility at SLS [24], were used to probe the crystal structure of $\text{Sr}_{0.97}\text{Ca}_{0.03}\text{TiO}_3$ after photoexcitation. A grazing incidence angle of $0.37 \pm 0.05^\circ$ was chosen to limit the x-ray probe depth (intensity) to ≤ 60 nm. The 110 fs p-polarized excitation pulse is centered around an energy of 4.66 eV to overcome the direct band gap (3.75 eV [25]) leading to an excitation depth of 18 nm. This results in an average photodoping of the probed volume of 0.01 eh-pairs per cubic unit cell for 1 mJ/cm² incident fluence. The crystal was cooled with a N_2 cryo-blower.

Figure 1 shows the normalized intensity of the (1.5 0.5 0.5) superlattice reflection as a function of the pump-probe delay for a series of excitation fluences ϕ taken at $T = 100$ K. A sudden reduction immediately after excitation is visible, followed by a subsequent slower decay during a few ps. For quantitative extraction of the time constants of the order parameter dynamics, we fit the normalized intensity by two exponential decays,

$$I = \left(1 - \Theta(t-t_0) \left[A_1 \left(1 - e^{-\frac{t-t_0}{\tau_1}}\right) + A_2 \left(1 - e^{-\frac{t-t_0}{\tau_2}}\right) \right] \right)^2$$

convolved with a 120 fs full-width at half-maximum Gaussian to account for overall experimental time-resolution. Θ is the Heaviside function, and A_1/τ_1 and A_2/τ_2 are the amplitude/decay constant values of the fast and slow decay components, respectively. Due to the mismatch between UV excitation and x-ray probe depth mentioned above, we base our discussion and conclusions solely on the decay constants. The fits result in a fast and slow decay constant of φ of approximately 0.2 ps and > 1 ps, respectively (see supplementary

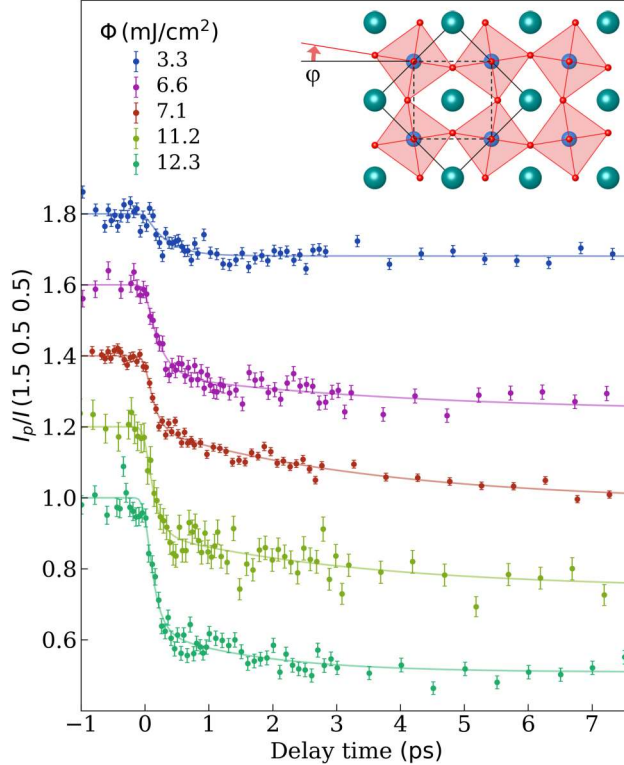


FIG. 1. Transient relative x-ray intensity of the (1.5 0.5 0.5) superlattice reflection of $\text{Sr}_{0.97}\text{Ca}_{0.03}\text{TiO}_3$ upon above bandgap excitation with 40 fs pulses centered around 4.66 eV at a temperature of 100 K. For clarity, a constant vertical offset of 0.2 separates traces recorded for different excitation fluences ϕ . Error bars indicate x-ray photon counting statistics. Inset: SrTiO_3 crystal structure as seen along the c -axis (Visualized using VESTA [23]). ϕ measures the antiferrodistortive rotation of the oxygen octahedra (exaggerated) and represents the order parameter. The dashed/solid black line frames a cubic/tetragonal unit cell of the high/low temperature phase along the respective in-plane axes.

material).

The slower decay component corresponds to the expected time scale for transfer of heat from the electronic system [15] to the lattice, so this component of the relaxation seems to be likely due to a simple temperature increase of the phonon system with the distortion following adiabatically. It is also possible that it is influenced by energy transport between the more excited near-surface region and the deeper regions of the sample.

The faster time scale is on the order of a half cycle period of the rotational mode at 100 K (2.5 THz, see supplementary material). However, when approaching T_c at 270 K the fast

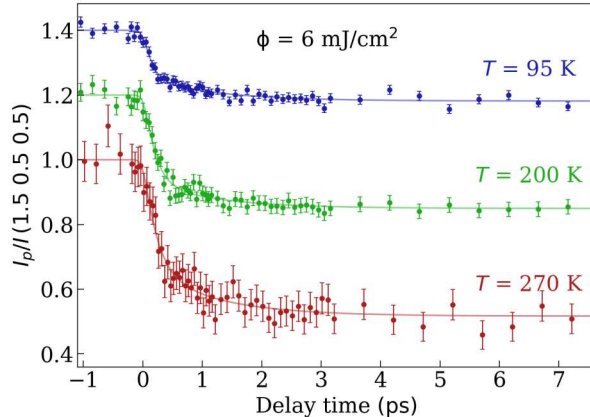


FIG. 2. Dynamics of the (1.5 0.5 0.5) superlattice reflection measured for temperatures approaching $T_c = 280$ K at an excitation fluence of $\phi = 6$ mJ/cm².

dynamics does not change significantly, which is in contrast to the increasing equilibrium soft mode period with temperature (0.8 ps at $T = 270$ K, see Fig. 2 and Fig. S2(b)). This points towards a non-adiabatic structural dynamics that is being driven by a faster than thermal modification of the structural soft-mode potential.

In principle, changes of the Debye-Waller factor imposed by optically induced lattice disordering can account for a strong reduction in the intensity of a Bragg peak on comparably fast timescales [26, 27]. In our case, a drop by 40% of the probed reflection would imply an average thermal isotropic atomic displacement by more than 60% of the cubic lattice constant. According to the Lindemann criterion, this would imply melting of the crystal lattice, which excludes such a scenario. As discussed in the supplementary material, we can also exclude a rapid order-disorder transition of the structural superlattice itself, i.e. a selective thermal dislocation of the 8h oxygen sites of the I4/mcm cell along the soft-mode coordinate.

For metallic systems with strong electron-lattice interaction, it has been shown that an ultrafast modification of the electronic population distribution can change the phonon potentials and non-thermally drive structural dynamics along zone-centered A_{1g} optical modes [28]. To explore whether photodoping across the band gap of an insulator can induce a non-thermal relaxation dynamics of a soft-mode driven distortion via a comparable mechanism, we model the photodoping process in SrTiO₃ from first principle calculations.

We first look into the effect of static doping on the phonon spectrum using density

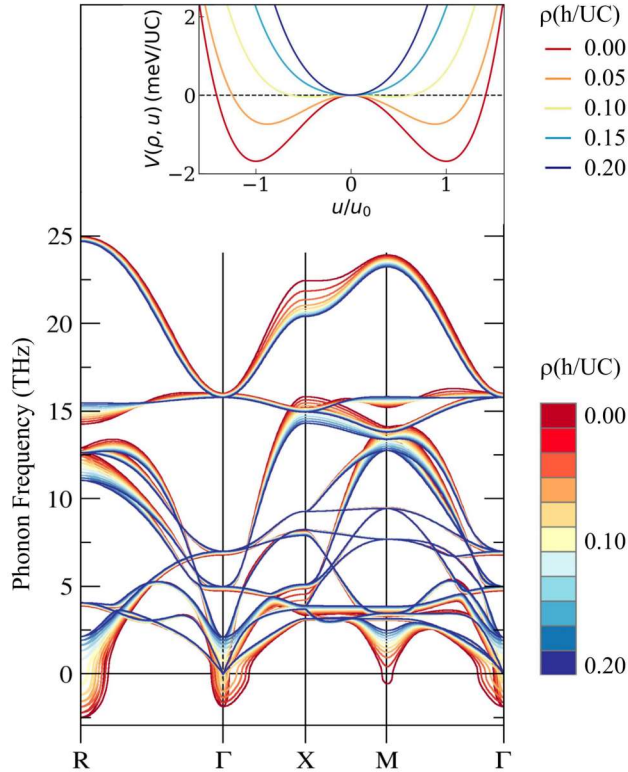


FIG. 3. DFT Phonon dispersion of cubic SrTiO₃ for a series of hole dopings (not including LO-TO splitting). Inset: Calculated energy change per SrTiO₃ cubic unit cell as a function of oxygen displacement u/u_0 along the in-plane cubic crystal axes resulting from the octahedral rotation at select hole dopings.

functional theory (DFT) [29] (VASP code). As a 3% Ca substitution does not qualitatively change the properties of the octahedral phase transition, we calculated the effect of hole doping on the phonon dispersion for pure SrTiO₃ following the approach for electron doping of Ref. [30]

In Fig. 3 we show the phonon dispersion of SrTiO₃ for different hole doping concentrations. Within the harmonic approximation, phonon modes with an imaginary frequency represent structural instabilities of a system. Without hole doping the spectrum exhibits phonon bands with imaginary frequencies (shown as 'negative' frequencies) around the R and Γ points. The instability at R represents the rotational low temperature ground state of SrTiO₃, whereas the one at Γ indicates its polar instability. Introduction of holes significantly shifts the lowest phonon bands upwards in energy, such that imaginary frequencies vanish at a critical concentration of 0.1 holes per unit cell. Consequently, hole doping sup-

presses rotational and polar instabilities and instead favors a cubic undistorted structure, in agreement with literature [31]. Electron doping, in contrast, does not induce this effect as rotational modes are almost unaffected [30].

Next, we quantify the potential energy landscape resulting from a modulation of the phonon at the R point by a harmonic double-well potential of the form

$$V(u, \rho) = \frac{\Omega(\rho)^2}{2}u^2 + \frac{\kappa(\rho)^2}{4}u^4 \quad (1)$$

where $\Omega(\rho)$ is the doping dependent phonon frequency and the second term with κ represents a higher order repulsive force. Minimizing Eqn. (1) gives the structural ground state, i.e. the octahedral rotational angle for each doping. The inset of Fig. 3 shows $V(\rho)$ for a series of doping values as a function of the oxygen displacement u relative to the optimal displacement at zero doping u_0 . The transformation of the double well to a single well potential for ρ above 0.1 h/UC reflects the stabilization of the cubic structure by doping.

To link the structure to the dynamic photodoping process, we replace the static doping ρ by a time-dependent hole concentration $\rho(t)$ which becomes a parametric driving force in Eqn. (1) that displaces u . The structural dynamics is then given by the equation of motion

$$\ddot{u}(t) + 2\gamma\dot{u}(t) + \nabla_u V(u(t), \rho(t)) = 0 \quad (2)$$

in which we account by $\gamma\dot{u}(t)$ for finite phonon lifetimes. We note that within this approach the interplay between $\rho(t)$ and $V(u, \rho)$ ultimately determines the dynamics of the structural distortion.

To account for a realistic transient doping $\rho(t)$ we next perform computations utilizing time-dependent DFT [32]. We hereby describe the photodoping process by the light pulse by including a time-dependent vector potential within our calculation. $\rho(t)$ is then determined by integrating the time-dependent density of holes at the top of the valence band, between $E_F - 0.2\text{eV}$ and E_F (which is in the vicinity of R), to capture only the hole states considered in the static calculation. Details of our calculations are presented in the supplementary part. Figure 4 shows an example timetrace of $\rho(t)$.

Having determined the transient doping $\rho(t)$ allows us to calculate the dynamics of the mode coordinate $u(t)$ by solving Eqn. (2). We show $u^2(t)$ as a function of time in Fig. 4. Here we use the damping γ of the soft mode obtained by ref. [33] extrapolated to $T = 120$ K. Note that the experiment captures a superposition of excitation intensities due

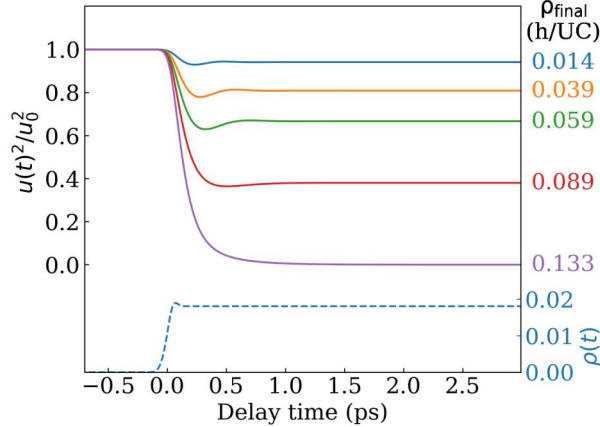


FIG. 4. Right y-axis: TDDFT simulation of the transient hole population $\rho(t)$ for excitation with a 110 fs field pulse centered 200 meV above the DFT bandgap (see Fig. S5). Left y-axis: Relative scattering intensity of superlattice peaks associated with the octahedral distortion, calculated via Eq. 2 for a parametric change of the double well potential of Fig. 3 by $\rho(t)$. The curves are labelled by the doping level ρ_{final} reached after the excitation process.

to the mismatch between excitation and probe depths (supplementary material). For a fluence of 3.3 mJ/cm², the calculated doping level close to the surface is 0.11 h/UC which is thus already sufficient to stabilize the cubic phase in part of the probed volume. In figure S6 we show the calculated transient reflection intensities with the influence of the profile mismatch taken into account using the model described in ref. [34]. The amplitude of the intensity drop obtained by the model is in a good overall agreement with the experimental amplitude of the fast decay component.

Most notably, we find that the timescale of the initial fast relaxation is qualitatively reproduced (Fig. 4 and Fig. S6). This shows that ultrafast modification of the soft-mode potential via photodoping of oxygen 2p valence holes can explain the observed fast relaxation of the structural order parameter. The following slower decay in the experimental data is not reproduced due to the absence of electron-phonon scattering in the model. Due to the nanosecond lifetime of photodoped e-h pairs [35], recombination processes are not expected to be relevant on the timescale of interest.

In conclusion, our time resolved study of the order parameter of a soft-phonon induced purely structural symmetry breaking transition demonstrates that optical excitation of the electronic system can induce a relaxation of the structural order parameter faster than

expected for lattice heating. Our results show that photodoping can modify the structural soft-mode potential and drive the order parameter, despite the equilibrium phase transition is not based on an electronic mechanism.

-
- [1] T. Rohwer, S. Hellmann, M. Wiesenmayer, C. Sohrt, A. Stange, B. Slomski, A. Carr, Y. Liu, L. M. Avila, M. Kalläne, S. Mathias, L. Kipp, K. Rossnagel, and M. Bauer, *Nature* **471**, 490 (2011).
 - [2] P. Beaud, A. Caviezel, S. O. Mariager, L. Rettig, G. Ingold, C. Dornes, S.-W. Huang, J. A. Johnson, M. Radovic, T. Huber, T. Kubacka, A. Ferrer, H. T. Lemke, M. Chollet, D. Zhu, J. M. Glowia, M. Sikorski, A. Robert, H. Wadati, M. Nakamura, M. Kawasaki, Y. Tokura, S. L. Johnson, and U. Staub, *Nat. Mater.* **13**, 923 (2014).
 - [3] S. Tomimoto, S. Miyasaka, T. Ogasawara, H. Okamoto, and Y. Tokura, *Phys. Rev. B* **68**, 035106 (2003).
 - [4] E. Möhr-Vorobeva, S. L. Johnson, P. Beaud, U. Staub, R. De Souza, C. Milne, G. Ingold, J. Demsar, H. Schaefer, and A. Titov, *Phys. Rev. Lett.* **107**, 036403 (2011).
 - [5] M. Porer, U. Leierseder, J.-M. Ménard, H. Dachraoui, L. Mouchliadis, I. E. Perakis, U. Heinzmann, J. Demsar, K. Rossnagel, and R. Huber, *Nat. Mater.* **13**, 857 (2014).
 - [6] A. Kirilyuk, A. V. Kimel, and T. Rasing, *Rev. Mod. Phys.* **82**, 2731 (2010).
 - [7] B. Koopmans, G. Malinowski, F. Dalla Longa, D. Steiauf, M. Fähnle, T. Roth, M. Cinchetti, and M. Aeschlimann, *Nat. Mater.* **9**, 259 (2010).
 - [8] H. Ehrke, R. I. Tobey, S. Wall, S. A. Cavill, M. Först, V. Khanna, T. Garl, N. Stojanovic, D. Prabhakaran, A. T. Boothroyd, M. Gensch, A. Mirone, P. Reutler, A. Revcolevschi, S. S. Dhesi, and A. Cavalleri, *Phys. Rev. Lett.* **106**, 217401 (2011).
 - [9] S. Johnson, R. De Souza, U. Staub, P. Beaud, E. Möhr-Vorobeva, G. Ingold, A. Caviezel, V. Scagnoli, W. Schlotter, J. Turner, *et al.*, *Phys. Rev. Lett.* **108**, 037203 (2012).
 - [10] T. A. Ostler, J. Barker, R. F. L. Evans, R. W. Chantrell, U. Atxitia, O. Chubykalo-Fesenko, S. El Moussaoui, L. Le Guyader, E. Mengotti, L. J. Heyderman, F. Nolting, A. Tsukamoto, A. Itoh, D. Afanasiev, B. A. Ivanov, A. M. Kalashnikova, K. Vahaplar, J. Mentink, A. Kirilyuk, T. Rasing, and A. V. Kimel, *Nat. Commun.* **3**, 666 (2012).
 - [11] L. Le Guyader, M. Savoini, S. El Moussaoui, M. Buzzi, A. Tsukamoto, A. Itoh, A. Kirilyuk,

- T. Rasing, A. V. Kimel, and F. Nolting, *Nat. Commun.* **6**, 5839 (2015).
- [12] A. Cavalleri, C. Tóth, C. W. Siders, J. A. Squier, F. Ráksi, P. Forget, and J. C. Kieffer, *Phys. Rev. Lett.* **87**, 237401 (2001).
- [13] V. R. Morrison, R. P. Chatelain, K. L. Tiwari, A. Hendaoui, A. Bruhács, M. Chaker, and B. J. Siwick, *Science (New York, N.Y.)* **346**, 445 (2014).
- [14] R. Cowley, *Adv. Phys.* **29**, 1 (1980).
- [15] J. Shah, in *Ultrafast Spectroscopy of Semiconductors and Semiconductor Nanostructures* (Springer, 1999).
- [16] G. Shirane and Y. Yamada, *Phys. Rev.* **177**, 858 (1969).
- [17] T. Riste, E. J. Samuelsen, K. Otnes, and J. Feder, *Solid State Commun.* **9**, 1455 (1971).
- [18] J. Kiat and T. Roisnel, *J. Phys.: Condens. Matter* **8**, 3471 (1996).
- [19] K. A. Müller and H. Burkard, *Phys. Rev. B* **19**, 3593 (1979).
- [20] Single crystals were obtained from surfaceNet GmbH, Germany.
- [21] P. R. Willmott, D. Meister, S. J. Leake, M. Lange, A. Bergamaschi, M. Böge, M. Calvi, C. Cancellieri, N. Casati, A. Cervellino, Q. Chen, C. David, U. Flechsig, F. Gozzo, B. Henrich, S. Jäggi-Spielmann, B. Jakob, I. Kalichava, P. Karvinen, J. Krempasky, A. Lüdeke, R. Lüscher, S. Maag, C. Quitmann, M. L. Reinle-Schmitt, T. Schmidt, B. Schmitt, A. Streun, I. Vartiainen, M. Vitins, X. Wang, and R. Wulschleger, *Journal of synchrotron radiation* **20**, 667 (2013).
- [22] S. K. Mishra, R. Ranjan, D. Pandey, P. Ranson, R. Ouillon, J.-P. Pinan-Lucarre, and P. Pruzan, *J. Solid State Chem.* **178**, 2846 (2005).
- [23] K. Momma and F. Izumi, *Journal of applied crystallography* **44**, 1272 (2011).
- [24] P. Beaud, S. L. Johnson, A. Streun, R. Abela, D. Abramsohn, D. Grolimund, F. Krasniqi, T. Schmidt, V. Schlott, and G. Ingold, *Phys. Rev. Lett.* **99**, 174801 (2007).
- [25] K. van Benthem, C. Elsässer, and R. H. French, *J. Appl. Phys.* **90**, 6156 (2001).
- [26] P. B. Hillyard, K. J. Gaffney, A. M. Lindenberg, S. Engemann, R. A. Akre, J. Arthur, C. Blome, P. H. Bucksbaum, A. L. Cavalieri, A. Deb, R. W. Falcone, D. M. Fritz, P. H. Fuoss, J. Hajdu, P. Krejčík, J. Larsson, S. H. Lee, D. A. Meyer, A. J. Nelson, R. Pahl, D. A. Reis, J. Rudati, D. P. Siddons, K. Sokolowski-Tinten, D. von der Linde, and J. B. Hastings, *Phys. Rev. Lett.* **98**, 125501 (2007).
- [27] A. M. Lindenberg, J. Larsson, K. Sokolowski-Tinten, K. J. Gaffney, C. Blome, O. Synnergren, J. Sheppard, C. Caleman, A. G. MacPhee, D. Weinstein, D. P. Lowney, T. K. Allison,

- T. Matthews, R. W. Falcone, A. L. Cavalieri, D. M. Fritz, S. H. Lee, P. H. Bucksbaum, D. A. Reis, J. Rudati, P. H. Fuoss, C. C. Kao, D. P. Siddons, R. Pahl, J. Als-Nielsen, S. Duesterer, R. Ischebeck, H. Schlarb, H. Schulte-Schrepping, T. Tschentscher, J. Schneider, D. von der Linde, O. Hignette, F. Sette, H. N. Chapman, R. W. Lee, T. N. Hansen, S. Techert, J. S. Wark, M. Bergh, G. Huldt, D. van der Spoel, N. Timneanu, J. Hajdu, R. A. Akre, E. Bong, P. Krejcik, J. Arthur, S. Brennan, K. Luening, and J. B. Hastings, *Science* **308**, 392 (2005).
- [28] D. M. Fritz, D. A. Reis, B. Adams, R. A. Akre, J. Arthur, C. Blome, P. H. Bucksbaum, A. L. Cavalieri, S. Engemann, S. Fahy, R. W. Falcone, P. H. Fuoss, K. J. Gaffney, M. J. George, J. Hajdu, M. P. Hertlein, P. B. Hillyard, M. Horn-von Hoegen, M. Kammler, J. Kaspar, R. Kienberger, P. Krejcik, S. H. Lee, A. M. Lindenberg, B. McFarland, D. Meyer, T. Montagne, É. D. Murray, A. J. Nelson, M. Nicoul, R. Pahl, J. Rudati, H. Schlarb, D. P. Siddons, K. Sokolowski-Tinten, T. Tschentscher, D. von der Linde, and J. B. Hastings, *Science* **315**, 633 (2007).
- [29] G. Kresse and J. Furthmüller, *Phys. Rev. B* **54**, 11169 (1996).
- [30] C. Cancellieri, A. S. Mishchenko, U. Aschauer, A. Filippetti, C. Faber, O. S. Barišić, V. A. Rogalev, T. Schmitt, N. Nagaosa, and V. N. Strocov, *Nat. Commun.* **7**, 10386 (2016), arXiv:1507.04723 [cond-mat.mtrl-sci].
- [31] K. Uchida, S. Tsuneyuki, and T. Schimizu, *Phys. Rev. B* **68**, 174107 (2003).
- [32] The elk LAPW code <http://elk.sourceforge.net>.
- [33] T. Kohmoto, K. Tada, T. Moriyasu, and Y. Fukuda, *Phys. Rev. B* **74**, 064303 (2006).
- [34] T. Huber, S. O. Mariager, A. Ferrer, H. Schäfer, J. A. Johnson, S. Grübel, A. Lübcke, L. Huber, T. Kubacka, C. Dornes, *et al.*, *Phys. Rev. Lett.* **113**, 026401 (2014).
- [35] H. Yasuda, Y. Yamada, T. Tayagaki, and Y. Kanemitsu, *Phys. Rev. B* **78**, 233202 (2008).

Ultrafast relaxation dynamics of the antiferrodistortive phase in Ca doped SrTiO₃

-Supplementary Information-

30.04.2018

M. Porer¹, M. Fechner^{2,3}, E. Bothschafter¹, L. Rettig^{1,6}, M. Savoini^{1,4}, V. Esposito¹, J. Rittmann^{1,5}, M. Kubli⁴, M. J. Neugebauer⁴, T. Kubacka⁴, T. Huber⁴, G. Lantz⁴, S. Parchenko¹, S. Grübel¹, E. Abreu⁴, A. Paarmann⁶, J. Noack⁷, P. Beaud^{1,5}, G. Ingold^{1,5}, U. Aschauer⁸, S. L. Johnson⁴, U. Staub¹

¹Swiss Light Source, Paul Scherrer Institute, 5232 Villigen-PSI, Switzerland

²Materials Theory, ETH Zürich, 8093 Zürich, Switzerland

³Max Planck Institute for the Structure and Dynamics of Matter, CFEL, 22761 Hamburg, Germany

⁴Institute for Quantum Electronics, ETH Zürich, 8093 Zürich, Switzerland

⁵SwissFEL, Paul Scherrer Institute, 5232 Villigen-PSI, Switzerland

⁶Department of Physical Chemistry, Fritz Haber Institute of the Max Planck Society, 14195 Berlin, Germany

⁷Department of Inorganic Chemistry, Fritz Haber Institute of the Max Planck Society, 14195 Berlin, Germany

⁸Department of Chemistry and Biochemistry, University of Bern, 3012 Bern, Switzerland

1. Structure factor of the (1.5 0.5 0.5) superlattice reflection

The structure factor F_{hkl} of the (1.5 0.5 0.5) superlattice reflection ((2 1 1) in the I4/mcm space group) of SrTiO₃ amounts to:

$$F_{\frac{3}{2}\frac{1}{2}\frac{1}{2}} = 4f_{O_2} \cdot (\sin(2\pi \cdot u) + \sin(6\pi \cdot u)) \approx 32\pi f_{O_2} u + \mathcal{O}(u^2)$$

with f_{O_2} the atomic form factor of the oxygen 8h sites and u the fractional lattice displacement in I4/mcm unit cell coordinates.

With $u \sim \varphi$, the intensity depends on u and φ as

$$I_{\frac{3}{2}\frac{1}{2}\frac{1}{2}} \propto F_{\frac{3}{2}\frac{1}{2}\frac{1}{2}}^2 \propto \varphi^2 + \mathcal{O}(\varphi^4)$$

This approximation of a square dependence holds for $\varphi \ll \pi/6$, which is given for realistic values of $\varphi \lesssim 0.035$ ($\sim 2^\circ$) [18].

2. Temperature dependence of the soft-mode frequency

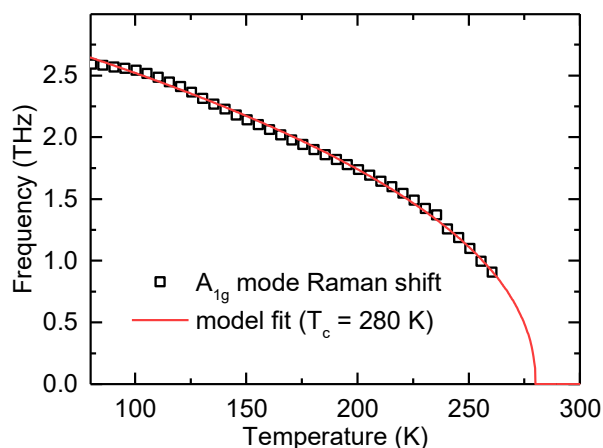


Figure S1 Frequency of the antiferrodistortive soft mode in Sr_{0.97}Ca_{0.03}TiO₃ as a function of temperature as measured by Raman spectroscopy. A power law fit reveals a critical temperature of $T_c = 280$ K for the structural phase transition. Measurements were performed at the Fritz Haber Institute, Berlin.

3. Fluence and temperature dependence of the fast relaxation time constant

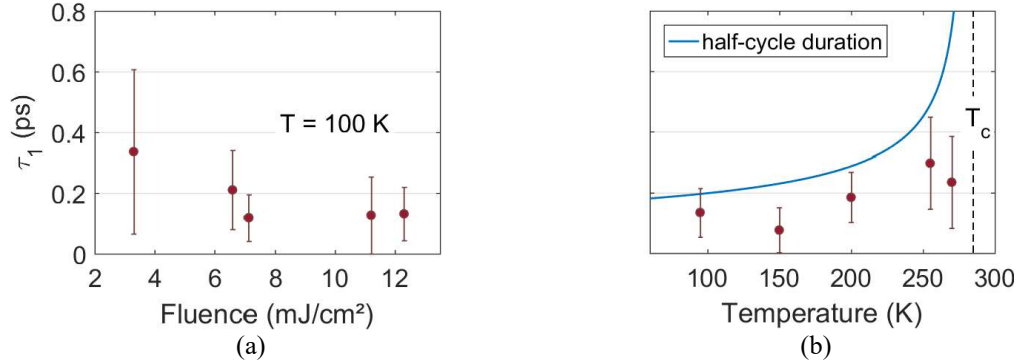


Figure S2 Fast decay time constant τ_1 of the lattice displacement u extracted from the dynamics of the (1.5 0.5 0.5) reflection intensity as (a) function of excitation fluence Φ at a $T = 100 \text{ K}$ and (b) as function of T at $\Phi = 6 \text{ mJ}/\text{cm}^2$.

4. Exclusion of an order-disorder transition scenario

As discussed in the main text, we can exclude a scenario in which the intensity reduction of the superlattice reflection can be attributed purely to the Debye-Waller factor of a thermally heated and equilibrated crystal lattice. For the structural transition studied here, one may further consider the implications of selective heating of the A_{1g} soft-mode or the oxygen 8h sites involved in the structural transition. Besides a favored population of the low frequency modes including the soft mode given by the Bose-Einstein statistics, depending on the mode-selective electron-phonon couplings, cooling of photoexcited carriers via phonon emission could in principle favor scattering into the soft mode branch. Such effects would lead to a temporarily increased thermal average displacement of the oxygen 8h sites that may rapidly reduce the intensity of the superlattice reflection and persist longer than captured by our experimental time window of a few picoseconds.

To test such a scenario, we reference the SL reflection intensity against the intensity of the structural (1 3 1) reflection, which exhibits a similar sensitivity to the thermal displacement of the 8h oxygens.

Figure S3 compares the expected influence of such thermal dislocation on the intensities of the superlattice (1.5 0.5 0.5) and the structural (1 3 1) reflections for two scenarios: First, we assume a O 8h dislocation approximately along the soft mode coordinate by elongating the thermal ellipsoid along the mode coordinate for small ϕ (left inset). Second, we assume an isotropic thermal displacement within the ab-plane (right inset). In either scenario, we find that a thermally induced reduction of the superlattice reflection (green curves) would imply a comparable drop in the measured structural reflection (red curves).

In our experiment, photoexcitation with $\Phi = 6 \text{ mJ}/\text{cm}^2$ yields no measurable change in the (1 3 1) reflection intensity within an error of 0.5% and in a time window of 5 ps after excitation.

Thus, we can exclude a scenario where the drop in the superlattice intensity can be attributed to a rapid thermal dislocation of the oxygen 8h sites, comparable to an order-disorder transition of the structural superlattice.

We note that dislocation of the oxygens along softened E_g modes [33] (oxygen motions along the c-axis) does not significantly affect the expected intensity of the superlattice reflection (not shown).

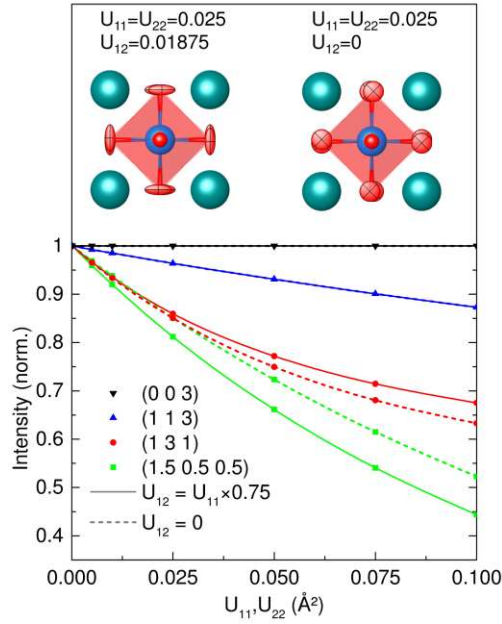


Figure S3 Expected intensity reduction of select x-ray reflections at 7.1 keV upon selective thermal heating. The abscissa represents the in plane thermal displacement of the oxygen 8h sites. All components of the other thermal ellipsoid $U_{ij(i \neq j)}$ are zero unless stated otherwise. Insets: Thermal ellipsoids (90% probability) of the 8h oxygen sites viewed along the c-axis for dislocation mainly along the soft mode coordinate (left) and isotropic within the ab-plane (right). Structure factor calculations and visualizations are performed with VESTA [23].

5. Doping dependence of the double-well potential coefficients

To determine the doping dependent coefficients of Eq. (1) we perform first-principle computations of the phonon band structure utilizing the approach and numerical setting of Ref. [30]. We determine the quadratic and quartic coefficients by modulating the structure along the eigenvector of the R-point phonon mode. By modulating the structure with the previously computed soft mode eigenvector we calculate the total energy of the system as a function of the mode amplitude. Finally, we fit the obtained energy landscape by a polynomial expression given in Eq. (1). In Fig. S4, we show the gained square and quartic coefficients as a function of doping. Whereas the quartic term is nearly unaffected by doping, we found a linear increase in the square factor.

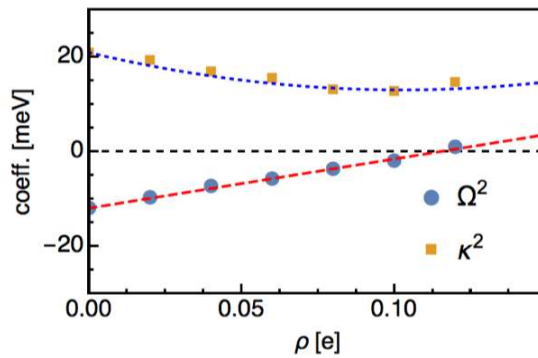


Figure S4: Change of the potential coefficients in Eq. (1) by hole doping.

6. Details of the TDDFT computations

We perform the TDDFT computations utilizing the implementations within the ELK code [32]. The electromagnetic field of the pump pulse is described by a time dependent vector potential.

We performed our computations for the cubic structure of SrTiO₃ with $a = 3.9 \text{ \AA}$ using as approximation for the exchange correlation functional the local density approximation (LDA). The numerical parameters for the time dependent computations have been fixed after thorough convergence tests. We use explicitly: $7 \times 7 \times 7$ k-point mesh to sample the Brillouin zone, a plane-wave cutoff within the interstitial of $|G + k|_{max} R_{MT}^{avg} = 7.5$ with the average muffin tin Radius $R_{MT}^{avg} = 0.98 \text{ \AA}$, we truncate the potential and density at $G_{max} = 20/a_0$, the maximum angular momentum for the local basis within the muffin tin is set to $l_{max} = 10$ for potential and wavefunction. Moreover, we add a total of 100 empty states to our basis to properly describe the excited states. For all not explicit listed parameters, we use the settings for high quality computations in Elk as triggered by “highq=.true.”.

Firstly, we perform a static regular DFT calculation of SrTiO₃ to determine its ground state electronic properties. Fig. S5 shows the electronic band structure of SrTiO₃ along selected symmetry lines within the first Brillouin zone. From this computation, we deduce the indirect LDA DFT band gap of SrTiO₃ to be 2 eV, which is lower than its experimental value of 3.25 eV [25]. Please note, that for the time-dependent calculation we have to take into account the deficiency of the LDA band gap to perform realistic computations.

We characterize the pump pulse in our computations by a Gaussian envelope pulse carrying a central frequency corresponding to 2 eV and with an FWHM of 80 fs. The amplitude of the pulse is adjusted to give similar fluence values a used in the experiment. Utilizing these values, we perform TDDFT computations, where we use time steps of 0.24 fs for solving the time-dependent Kohn-Sham equations. Within these calculations, we take a snapshot of the time-dependent density of states projected on the equilibrium ground-states after each five-time steps. Integration of these curves close to the Fermi energy gives the time-dependent hole concentration.

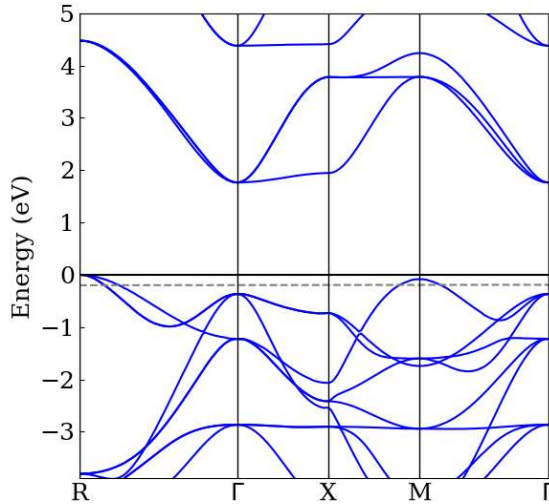


Figure S5 Band structure of cubic SrTiO₃ as calculated via the elk FP-LAPW code. The dashed horizontal line indicates the integration range for $\rho(t)$ induced by the TDDFT field pulse. Please note that the Fermi energy corresponds to 0 eV.

7. Simulated dynamics including x-ray and laser parameters

To account for the mismatch in the experimental excitation and probe profiles, we calculate $u^2(t)/u_0^2$ for a series of layers from the surface into the bulk crystal with depth-dependent doping given by the excitation profile. We then superimpose $u^2(t)/u_0^2$ of the individual layers weighted by the x-ray probe profile [34]. Furthermore, we account for the experimental x-ray pulse duration by convolution with a Gaussian (FWHM 120 fs). Figure S6 shows the resulting transient intensities for selected fluences used in the experiment.

We note that strongly damped coherent oscillations of $u(t)$ (Fig. 4) do not transfer to the resulting transient intensity due to the superposition of various oscillation frequencies given by the layer dependent excitation intensity / soft mode frequency.

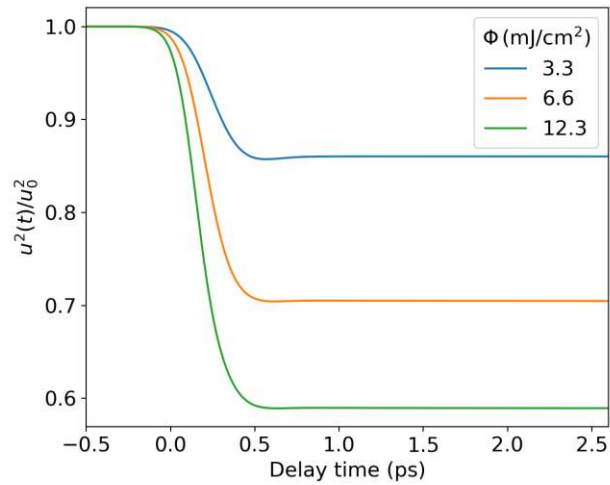


Figure S6 Simulated dynamics of the normalized intensity of a superlattice reflection taking into account the penetration depth of the pump intensity (18 nm), the x-ray probe depth (60 nm) and x-ray pulse duration (120 fs).